HHS Public Access

Author manuscript

ACS Appl Mater Interfaces. Author manuscript; available in PMC 2021 September 02.

Published in final edited form as:

ACS Appl Mater Interfaces. 2020 September 02; 12(35): 38887–38898. doi:10.1021/acsami.0c07206.

Systematic Study of Perfluorocarbon Nanoemulsions Stabilized by Polymer Amphiphiles

Rachael A. Day,
Department of Chemistry and Biochemistry, University of California, Los Angeles, Los Angeles, California 90095, United States

Daniel A. Estabrook,
Department of Chemistry and Biochemistry, University of California, Los Angeles, Los Angeles, California 90095, United States

Carolyn Wu,
Department of Chemistry and Biochemistry, University of California, Los Angeles, Los Angeles, California 90095, United States

John O. Chapman,
Department of Chemistry and Biochemistry, University of California, Los Angeles, Los Angeles, California 90095, United States

Alyssa J. Togle,
Department of Chemistry and Biochemistry, University of California, Los Angeles, Los Angeles, California 90095, United States

Ellen M. Sletten
Department of Chemistry and Biochemistry, University of California, Los Angeles, Los Angeles, California 90095, United States

Abstract

Perfluorocarbon (PFC) nanoemulsions, droplets of fluorous solvent stabilized by surfactants dispersed in water, are simple yet versatile nanomaterials. The orthogonal nature of the fluorous phase promotes the formation of nanoemulsions through a simple, self-assembly process while simultaneously encapsulating fluorous-tagged payloads for various applications. The size, stability, and surface chemistry of PFC nanoemulsions are controlled by the surfactant. Here, we systematically study the effect of the hydrophilic portion of polymer surfactants on PFC nanoemulsions. We find that the hydrophilic block length and identity, the overall polymer

Corresponding Author: **Ellen M. Sletten –** sletten@chem.ucla.edu.

Author Contributions

The manuscript was written through contributions of all authors. All authors have given approval to the final version of the manuscript.

Supporting Information

The Supporting Information is available free of charge at https://pubs.acs.org/doi/10.1021/acsami.0c07206.

Supporting schemes; supporting figures; general experimental procedures; figure experimental procedures; supporting figure experimental procedures; polymer characterization; ^{1}H NMR of the polymer library; and size exclusion chromatography (SEC) of the polymer library (PDF)

Complete contact information is available at: https://pubs.acs.org/10.1021/acsami.0c07206

The authors declare no competing financial interest.

hydrophilic/lipophilic balance, and the polymer architecture are all important factors. The ability to modulate these parameters enables control over initial size, stability, payload retention, cellular internalization, and protein adsorption of PFC nanoemulsions. With the insight obtained from this systematic study of polymer amphiphiles stabilizing PFC nanoemulsions, design features required for the optimal material are obtained.

Graphical Abstract

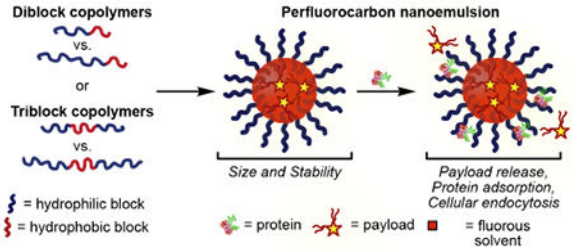

Keywords

perfluorocarbon nanoemulsion; polymer amphiphile; poly(2-oxazoline); stability; payload release; protein corona; endocytosis

INTRODUCTION

Nanomaterials have been extensively studied for use as drug delivery vehicles because of their ability to transport insoluble cargoes, protect sensitive therapeutics, increase circulation times, and allow for targeted delivery and release.[1,2] Numerous nanomaterial scaffolds have been developed, ranging from hard inorganic particles to soft materials.[3] Despite decades of work on nanodelivery vehicles, several challenges remain in this field including (1) protein corona formation impeding targeted molecular recognition, (2) difficulties regulating cellular internalization, and (3) imprecise payload delivery.[4–6] Systematic studies of subclasses of nanomaterials have provided insight into these challenges[7–12] and have revealed that the core nanomaterial structure significantly influences the interactions of the nanomaterials with biomolecules.[7,13–15] Thus, for each new class of nanomaterial, a thorough investigation of structure–property relationships is required.

To date, soft nanomaterials such as liposomes, polymer micelles, and emulsions have had the most success regarding clinical translation.[16,17] These nanomaterials rely on self-assembly of amphiphiles, with liposomes and polymer micelles being solely composed of amphiphiles while emulsions contain an oil phase that is stabilized by the amphiphiles (i.e., surfactants) in water. Nanoemulsions are kinetically stable, and large amounts of cargo can be loaded into them, giving nanoemulsions advantages over liposomes and micelles that are prone to disassembly at low concentrations.[18,19] However, applications of emulsions in controlled drug delivery have been hindered by leakage of therapeutics from the emulsion core to surrounding hydrophobic environments.[20,21] We aim to overcome this limitation of nanoemulsions by employing an oil phase composed of bioorthogonal perfluorocarbons (PFCs) rather than traditional hydrocarbon oils. Using this approach, payloads can be

localized in PFC nanoemulsions by the use of fluorous tags (Figure 1A). The matched solubility of fluorous-solubilized payloads in PFC nanoemulsions decreases the leaching of the payloads significantly when compared to traditional hydrophobic analogues,[22] allowing the advantageous stability and high cargo loading characteristic of emulsions to be capitalized upon.

PFCs, molecules in which all C–H bonds have been replaced with C–F bonds, have unique properties. They phase separate from aqueous and organic solutions to form a dense fluorous phase.[23] The fluorous phase has high gas solubility which led to the first biomedical application of PFC nanoemulsions as blood substitutes, where Pluronic polymer amphiphiles were employed as surfactants to stabilize PFCs in water.[24,25] In the decades since, PFC nanoemulsions have been used for ^{19}F-MRI,[26–28] as ultrasound contrast agents,[29,30] and as intracellular sensors,[31] with both small-molecule and polymeric surfactants stabilizing the droplets. Research has shown that PFC nanoemulsions are endocytosed by cells,[32,33] and the surfactant can dictate the mechanism of endocytosis.[34] However, a systematic study of the effect of the amphiphile on PFC nanoemulsion stability, payload retention, protein corona formation, and cellular internalization has yet to be performed. This knowledge is essential to advance the utility of PFC nanoemulsions as therapeutic and diagnostic nanocarriers.

Previously, we have investigated poly(2-oxazoline) (POx) amphiphiles as surfactants for PFC nanoemulsions rather than the Pluronic surfactants that were originally employed for oxygen delivery.[35] Our interest in POx stems from their controlled ring opening polymerization, ease of functionalization through incorporation of co-monomers or end-capping, and commercially available monomer starting materials. POx polymers have been utilized in protein polymer conjugates, grafted onto liposomal bilayers, formulated into micelles, applied to surfaces, and are validated alternatives to poly- (ethylene glycol) (PEG).[36,37] PEGylation has been widely successful at lengthening serum half-lives and minimizing protein coronas; however, its extensive use has led to immunogenicity concerns. Thus, in the next iteration of nanomaterials, alternatives to PEG (and Pluronics) are desirable.[36] In our initial work exploring POx surfactants for nanoemulsions, we focused on variations in the hydrophobic portion of POx amphiphiles and found that poly(2-nonyl-2-oxazoline) [P(NonOx)] outperformed either poly(2-propyl-2-oxazoline) or a fluorous-containing oxazoline.[38] Here, we systematically look at the role of the hydrophilic block in custom polymeric amphiphiles and readily available commercial PEG-containing surfactants for their ability to stabilize PFC nanoemulsions over time (Figure 1B). Subsequently, we analyze their effect on payload retention, protein corona formation, and cellular internalization (Figure 1C).

RESULTS AND DISCUSSION

Inspired by commercial Pluronic and Zonyl surfactants (**1–4**, Figure 2A), we synthesized a library of diblock and triblock amphiphiles (**5–16**, Figure 2B). Both diblock and triblock copolymers (DBCs and TBCs) stabilize the water–PFC interface; however, their mechanisms differ with the diblock surfactants having the hydrophobic block extended into the oil phase, whereas the triblock surfactants create a U shape with the majority of the hydrophobic block positioned at the interface.[38–40] In both cases, the hydrophilic block

extends out into the aqueous media, thus dictating the surface properties and ultimately contributing to the biodistribution of the PFC nanoemulsions. Notably, in previous works, we found distinct differences in nanoemulsion stability when the repeating unit of the polymer was altered or when the architecture of the surfactants was changed from diblock to triblock.[38] These results prompted the inclusion of different amphiphile structures and architectures in this study.

POx polymers were synthesized via microwave-assisted cationic ring-opening polymerizations[41] employing methyl triflate as the initiator and quenching with water (Scheme S1A). Due to the living nature of the polymerization, the block lengths can be finely tuned by adjusting the initiator to monomer ratio.[42] The block lengths have been rounded for simplicity, with exact block lengths given in the Supporting Information. The polymer amphiphiles were synthesized in either an AB (**5–8**, **11–13**) or ABA (**9–10**) fashion, where A was either poly(2-methyl-2-oxazoline) [P(MeOx)] (**5–10**) or poly(2-ethyl-2-oxazoline) [P(EtOx)] (**11–13**), as both these polymers have been utilized as PEG replacements. The B block is hydrophobic poly(2-nonyl-2-oxazoline) [P(NonOx)] (Figure 2B), which was chosen based on our previous studies.[38]

Hybrid amphiphiles **14–16** were also prepared with PEG as the hydrophilic block and P(NonOx) as the hydrophobic block by initiating P(NonOx) synthesis directly from the PEG chain (Scheme S1B). Polymers **14–16** were prepared to aid in comparisons between the synthetic POx polymers (12 total) and four commercial polymers containing PEG A blocks: Pluronic F-68, Pluronic F-127, Zonyl FSO, and Zonyl FSN (**1–4**). The Pluronics were chosen because of their previous success as the FDA-approved surfactants for PFC nanoemulsions.[43] The Zonyl surfactants were investigated as an alternative commercial PEG-containing block copolymer that has previously been employed for PFC nanoemulsion formation.[44,45] It should be noted that the Zonyl surfactants have a fluorous B block and significantly shorter PEG A blocks than other amphiphiles in this study.

Size and Stability.

To study the size and stability of PFC nanoemulsions stabilized by the synthetic and commercial amphiphiles, the optimal concentration of the polymer was investigated for selected surfactants. Polymer surfactants, ranging from 28 mg/mL (2.8 wt %) to 3.5 mg/mL (0.35 wt %), were dissolved in water, added to fluorous solvent [7:3 perfluorodecalin (PFD)/perfluorotripropylamine (PFTPA)] (20 μL, 10 vol %), and sonicated (90 s, 35% amp) to form nanoemulsions (Figure S1). The size and polydispersity index (PDI) were analyzed via DLS. In most cases, emulsions containing 28 mg/mL polymer were smaller and had lower dispersities, showing that more uniform droplets were obtained.

With this knowledge in hand, emulsions stabilized by selected surfactants were prepared utilizing perfluorooctyl bromide (PFOB), perfluoro-15-crown-5-ether (PFCE), or 7:3 PFD/PFTPA as the fluorous phase (Figure 2C,D). PFOB and PFCE are commonly employed for ^{19}F MRI,[26,27] while 7:3 PFD/PFTPA represents the mixture that was FDA-approved for oxygen delivery.[46] The size and stability data are grouped by the surfactant type: commercial (blue), P(MeOx) (red), P(EtOx) (green), and PEG$_n$-*b*-NonOx$_{10}$ (orange). From the data in Figure 2C,D, it is clear that the initial size and stability of PFC nanoemulsions are

dependent on both the polymer amphiphiles and the molecular structure of the PFC. These results are consistent with those recently published by Mecozzi and co-workers,[47] demonstrating that the use of PFCE as the oil phase results in more stable emulsions than those formed from PFD, and emulsions composed of PFOB experience similar levels of Ostwald ripening across all polymer amphiphiles. To study the effect of the polymer amphiphiles, we employed 7:3 PFD/PFTPA, as this mixture displayed the largest differences between each surfactant in both the size and stability.

Nanoemulsions were then formulated with the panel of surfactants (**1–16**) at a concentration of 28 mg/mL (2.8 wt %). The hydrodynamic diameter was monitored immediately after formation (Figure 2E) and subsequently, for 30 days (Figure 2F). To minimize micelle formation, all P(MeOx) and P(EtOx) containing polymers (**5–13**) were first dissolved in dimethyl formamide (DMF) before dilution with water and addition of the fluorous solvent. PEG_{π}-*b*-$NonOx_{10}$ (**14–16**) were first dissolved in DMF, tetrahydrofuran (THF), and methanol (MeOH), respectively, to fully solubilize the polymer.

The size and stability data are grouped by the surfactant type; in addition, the DBCs (solid) are differentiated from the TBCs (diagonal stripes). The stability data in Figure 2F are represented by the change in the volume of the droplets over 30 days, and raw data can be found in Figure S2. The main pathway for destabilization of PFC nanoemulsions is Ostwald ripening, defined as a gradual increase in size over time as the solvent in the smallest droplets migrates to larger droplets.[18] Factors that affect Ostwald ripening are sample polydispersity, concentration, presence of micelles, and identity of PFC.[47,48]

A universal trend observed in all polymers tested was the longer the hydrophilic block, the larger the droplets were on day zero. Looking at the commercial PEG-containing polymers, we found that they all stabilize emulsions of similar size yet have varied stability over 30 days. Pluronic F-68 (**1**), which was employed in the original FDA-approved blood substitute formulation, has the worst stability of the four commercial amphiphiles tested, with the diblock fluorosurfactant Zonyl FSN (**4**) displaying the best stability. This could be due to the relative lipophilicities of the B block within the Pluronic and Zonyl surfactants. The B block of the Pluronic series is poly(propylene oxide) which is insoluble in water, with limited solubility in PFC oils, resulting in rejection anchoring to the fluorous solvent in contrast to the Zonyl surfactants containing a fluorous B block.[49] The Pluronic F-68 (**1**) nanoemulsions represent a good stability metric, as one of the reasons the FDA-approved formulation was removed from the market was inconsistencies in the formulation because of low stability.[43,50] Over 30 days, the Pluronic F-68 (**1**) emulsions increased in volume 1×10^7 nm^3, with the other commercial surfactants (**2–4**), the P(MeOx) tri-block (**10**), P(EtOx) (**11** and **13**), and PEG_{π}-*b*-$NonOx_{10}$ (**14** and **16**) displaying similar or superior stability.

For the P(MeOx) series (**5–7**), as the hydrophilic block increased, there was an apparent decrease in stability over 30 days when the P(NonOx) block was kept constant at approximately 10 repeat units (volume increase of 1.7×10^7, 2.2×10^7, 2.7×10^7 nm^3). When the P(NonOx) block was lengthened to approximately 30 repeat units, we found that P($MeOx_{90}$-*b*-$NonOx_{30}$) (**8**) has similar stability to P($MeOx_{30}$-*b*-$NonOx_{10}$) (**5**), suggesting that for diblock surfactants the overall hydrophilic/lipophilic balance (HLB) is a critical

metric (Figure S3). Notably, the TBCs ABA surfactants, P($MeOx_{30}$-*b*-$NonOx_{10}$-*b*-$MeOx_{30}$) (**9**) and P($MeOx_{90}$-*b*-$NonOx_{30}$-*b*-$MeOx_{90}$) (**10**) which have the same HLB, do not behave similarly, with **9** giving smaller initial size but showing significant Ostwald ripening over 30 days (2.8×10^7 nm^3 increase), while **10** displays excellent stability (0.5×10^7 nm^3 increase). We attribute the 30 day stability difference between **9** and **10** to larger A blocks favoring the steric stabilization method of TBCs.[40,49] Of the P(MeOx) polymers, P($MeOx_{30}$-*b*-$NonOx_{10}$) (**5**) diblock and the P($MeOx_{90}$-*b*-$NonOx_{30}$-*b*-$MeOx_{90}$) (**10**) triblock amphiphiles are the most promising if stability is desired.

The P(EtOx) series displays similar trends of initial size increase as the A block is lengthened. The P(MeOx) stability trends can be applied to the P(EtOx) series in which P($EtOx_{30}$-*b*-$NonOx_{10}$) (**11**) and P($EtOx_{90}$-*b*-$NonOx_{30}$) (**13**) DBCs have equivalent HLB and similar stabilities (volume increase of 0.3×10^7 vs 0.15×10^7 nm^3). These two P(EtOx) amphiphiles displayed superior overall stability to the P(MeOx) amphiphiles, showing that both P(MeOx) and P(EtOx) are viable monomers for amphiphiles to stabilize PFC nanoemulsions. Both the HLB and the overall amphiphile structure are important parameters.

Finally, looking at the use of PEG as the hydrophilic block and P(NonOx) as the hydrophobic block (**14–16**), we observe similar sized nanoemulsions with variable stability. The shortest PEG chain with 22 repeat units as the A block (**14**) led to the most stable emulsions over time, with all PEG_n-*b*-$NonOx_{10}$ stabilized emulsions (**14–16**) displaying superior or equivalent stability compared to the commercial PEG-containing surfactants.

Collectively, from these size and stability data, we conclude that the HLB (Figure S3) is a good metric for predicting if DBC amphiphiles will lead to stable PFC nanoemulsions ($<1 \times 10^7$ nm^3 increase in volume). For TBCs, sterics of the hydrophilic block (i.e. length of the A block) is a better predictor of stability than HLB.

Payload Retention.

The ideal nanomaterial allows for control of payload release. The advantage of PFC nanoemulsions over traditional oil emulsions is that the orthogonal nature of the fluorous phase gives a chemical handle to control the loading of different payloads inside the droplets through the use of fluorous tags.[51] Previously, we have established a relationship between the fluorous tag on the payload and retention in the droplets.[52,53] Here, we assayed the role of the surfactant in payload release by analyzing emulsions containing a consistent payload, fluorous-tagged coumarin **17**. Ultimately, multiple methods to control the release profiles of payloads are desirable. Our goal is to develop PFC nanoemulsions that can be applied to a wide array of diseases and patients. In some instances, slow release will be essential while in others, complete payload delivery over a few days may be desirable.

To test the retention of the payload in the PFC nanoemulsions, diluted aqueous solutions of droplets stabilized by surfactants **1–16** containing coumarin were rocked against 1-octanol, a known cell membrane mimic[54] (Figure 3A). The fluorescence of 1-octanol, which corresponded to coumarin leached from the nanoemulsions, was monitored to determine the percent release of the dye. It is immediately apparent looking at the payload release data in

Figure 3B that the surfactant plays a significant role in payload retention. When comparing the three hydrophilic blocks [P(MeOx), P(EtOx), and PEG], the P(MeOx) block (polymers **5–10**, red) displays superior payload retention. We hypothesize that this is due to the increased hydrophilicity of P(MeOx) over PEG and P(EtOx),[36] which minimizes the interaction of the nanoemulsions with the 1-octanol layer, retarding the leakage of the coumarin. The largest variability in release is observed with the PEG polymers, where a clear trend with the molecular weight is observed. The Pluronics (**1**, **2**, blue) have the largest PEG content and retain over 90% of their cargo over 14 days, while the Zonyls (**3**, **4**, blue) which have short PEG blocks of 4–12 repeat units release 30% of their cargo within 3 days. Looking at the hybrid PEG_n-*b*-$NonOx_{10}$ amphiphiles (**14–16**), it is evident that a larger PEG chain is advantageous for cargo retention as PEG_{1K}-*b*-$NonOx_{10}$ (**14**) displays the worst retention of all polymers tested (74% coumarin loss after 3 days), while PEG_{5K}-*b*-$NonOx_{10}$ (**16**) only loses 20% of the payload after 3 days. We attribute this molecular weight trend to the increased hydrophilicity and steric protection of longer hydrophilic blocks at the interface, minimizing interactions of the droplets with the 1-octanol layer.[55,56]

From these data, it appears that leaching of payload from PFC nanoemulsions can be attributed to the hydrophilicity and sterics of the studied amphiphiles (Figure S3). The increased hydrophilicity, either by tuning innate hydrophilicity [PEG and P(EtOx) vs P(MeOx)] or by increasing block length (PEG_{1K} vs PEG_{5K}) decreases the overall leakage of fluorous payloads. If a nanomaterial is desired that will not release its payload, the P(MeOx) series is far superior. If slow release of payload over time is necessary, Zonyl, P(EtOx), or PEG_{5K}-*b*-NonOx would be appropriate choices.

Cellular Uptake.

Next, we analyzed the effect of the surfactant on the cellular uptake of the PFC nanoemulsions. It is well established that nanomaterials, including PFC nanoemulsions, are most often internalized via endocytosis.[31,32] Previously, we have shown that nanoemulsions stabilized by Pluronic F-68 (**1**) and P($MeOx_{30}$-*b*-$NonOx_{10}$) (**5**) loaded with a fluorous soluble rhodamine[52] displayed colocalization with LysoTracker in phagocytic and nonphagocytic cell lines when analyzed by confocal microscopy.[38] We performed analogous experiments with surfactants **1, 5–6, 11**, and **16**, which all displayed robust colocalization with LysoTracker (Figures S4–S6). Representative images with **6** [P($MeOx_{60}$-*b*-$NonOx_{10}$)], **11** [P($EtOx_{30}$-*b*-$NonOx_{10}$)], and **16** (PEG_{5K}-*b*-$NonOx_{10}$) are displayed in Figure 4A, showing that the molecular structure of the hydrophilic block does not affect the cellular localization of the PFC nanoemulsions.

Despite all PFC nanoemulsions being internalized by endocytosis, we hypothesized that the varying surface chemistry may cause differences in the dominant pathway of endocytosis. To test this, we further explored the mechanism of endocytosis through treatment with common inhibitors for clathrin-mediated (chlorpromazine), caveolin-mediated [methyl-β-cyclodextrin (MβCD)], macropinocytosis (wortmannin), micropinocytosis (sodium azide), and energy-dependent pathways (sodium azide, temperature) (Figure 4B).[4,5,57–59] We used the macrophage cell line RAW264.7 for these studies, as it is the most well-characterized cell line with the chosen panel of inhibitors. To explore different endocytosis pathways, RAW

cells were incubated in basal media for 1 h with each respective inhibitor. PFC nanoemulsions containing a fluorous soluble rhodamine label[52] were added and incubated for an additional 3 h at 37 °C. For cells at 4 °C, emulsions were added and incubated for 1 h, to minimize cell death (Figure S7). Following incubation, the cells were washed to remove excess emulsions. The cells were then imaged (Figures S8 and S9) or analyzed via flow cytometry (Figures 4C–F and S10–S12). The data suggest that all commercial (**1–4**, blue) and P(MeOx) (**5–10**, red) emulsions are internalized through a clathrin-mediated process as shown by the 30–70% decrease in cellular uptake in the presence of chlorpromazine (Figure 4C,D horizontal stripes). For more hydrophobic polymers P(EtOx) (**11–13**, green) and PEG_{π}-*b*-$NonOx_{10}$ (**14–16**, orange), chlorpromazine had much less of an effect, causing only a 20% decrease in uptake (Figure 4E,F). Wortmannin and MβCD (Figure S10) had minimal effect on the uptake of all PFC nanoemulsions, indicating that they are not internalized via caveolin or micropinocytosis pathways. Sodium azide (NaN_3, vertical stripes) did not affect the commercial (**1–4**) or P(MeOx) (**5–10**) but caused a 20% decrease in the uptake of P(EtOx) (**11–13**) and PEG_{π}-*b*-$NonOx_{10}$ (**14–16**) emulsions. Chloroquine (diagonal stripes), most commonly used as an endosomal escape agent,[60] has also been shown to inhibit clathrin-mediated endocytosis[61] and decreased uptake of all nanoemulsions by 20–30%. For all polymers, lowering the temperature drastically affected the uptake, leading to a decrease of 80–90%, indicating that internalization is an energy-dependent process for all the PFC nanoemulsions assayed. For the commercial (**1–4**) and the P(MeOx) (**5–10**) polymers, clathrin-dependent endocytosis is the prominent route as shown by the >40% decrease in uptake when chlorpromazine is present. However, the P(EtOx) and the PEG_{π}-*b*-$NonOx_{10}$ polymers appear to be endocytosed by a combination of pathways allowing for uptake of PFC nanoemulsions through either clathrin-mediated or macropinocytosis-mediated pathways.

To support that the differences in uptake observed for emulsions stabilized by different surfactants is due to the surfactant identity and not differences in the emulsion sizes, nanoemulsions of consistent surfactants yet different sizes were prepared by altering the weight percent of the amphiphile employed during emulsion formation. Using this approach, emulsions of 150–300 nm in diameter were prepared from P($MeOx_{30}$-*b*-$NonOx_{10}$) (**5**) (Figure S13). RAW cells were treated with or without chlorpromazine followed by emulsions of different sizes, and the degree of uptake was assayed by flow cytometry. We found that uptake was universally reduced by 50% upon treatment with chlorpromazine, suggesting that any size differences between the emulsions did not significantly affect cellular uptake (Figure S13).

Protein Adsorption.

POx polymers have been used to replace PEG as a non-immunogenic, anti-biofouling alternative for surfaces,[62,63] protein conjugates,[36,64] and nanomaterials.[65,66] When nanomaterials come into contact with biological materials, protein adsorbs to the surface, forming a protein corona that masks the molecular identity of the material.[6] This corona alters the interaction of the nanomaterials and cells, which has been reported to influence routes of endocytosis.[4–6]

POx polymers have been reported to repel proteins more effectively than PEG when conjugated to nanomaterials.[67,68] We looked to investigate if this trend was consistent for nanoemulsions stabilized by POx and PEG amphiphiles. To assay the relative protein adsorption on PFC nanoemulsions stabilized by surfactants (**1–16**, Figure 5A), emulsions were prepared and treated with bovine serum albumin (BSA, Figures 5B and S14), cell culture media containing FBS (Figure 5C), or 10% human serum in PBS (Figure S15). First, emulsions were rocked against a BSA solution for 2 h and washed, and any isolated protein was precipitated and quantified via Bradford assay (Figure 5B). The results of the Bradford assay indicate that there is little difference in total protein adsorption between nanoemulsions stabilized by polymer surfactants containing PEG, P(MeOx), and P(EtOx) hydrophilic blocks. We further analyzed the protein adsorption by sodium dodecyl sulfate polyacrylamide gel electrophoresis (SDS-PAGE) analysis. For these experiments, surfactants (**14, 5–12**, and **14–15**) were treated with media containing FBS and subjected to the same procedure as described above. SDS-PAGE analysis indicates that all nanoemulsions adsorb BSA present in media (65 kDa protein); however, differences are observed in the minor proteins present in FBS. Nanoemulsions stabilized by amphiphiles **11** and **12** containing P(EtOx) hydrophilic blocks displayed significant adsorption of the IgG light chain (25 kDa protein). Alternatively, emulsions stabilized by PEG or P(MeOx) DBC showed more adsorption of low molecular weight proteins insulin (10 kDa) and cytochrome *c* (12 kDa). Thus, the SDS-PAGE analysis suggests that the identity of the hydrophilic block is able to alter the proteins within the corona, even if the overall magnitude of the protein adsorbed is similar. The identity of proteins adsorbed to the nanomaterial surface has been implicated in promoting the stealth effect through the avoidance of the mononuclear phagocyte system *in vivo.*[69,70]

After studying the protein corona formed on PFC nanoemulsions *in vitro,* we were interested in the effect that the adsorbed protein would have on cellular uptake (Figure 6A). To study this, emulsions were treated with either PBS or BSA before being added to RAW cells. After 3 h, the cells were washed and analyzed by flow cytometry. We found that the presence of BSA affected the overall uptake of nanoemulsions stabilized by **1**, **9**, **11,** and **16** but not **5** or **6** (Figure 6A). The nanoemulsions showed no significant difference in size or fluorescence (Figure S16), suggesting that these results are due to varied amphiphiles. To further analyze the effect of the protein corona on cellular uptake, we treated RAW cells with media, emulsions, and the cellular internalization inhibitors tested in Figure 4. The presence of BSA showed no effect on the route of endocytosis (Figures 6B and S17), indicating that the presence of protein does not influence the mechanism of internalization.

CONCLUSIONS

In this work, we utilized a polymer library to investigate the effect of polymer amphiphiles on stabilizing PFC nanoemulsions through the systematic variation of the hydrophilic block of the surfactants. From this study, when determining the best polymer amphiphile to stabilize nanoemulsions, the length of the A block, the HLB, the polymer architecture, and the molecular identity should be considered. Each of these properties plays a role in the initial size, stability, payload retention, cellular endocytosis, and protein adsorption of PFC

nanoemulsions. We envision that these design principles can be applied to other polymer amphiphile-stabilized nanoemulsion systems.

The initial size of PFC nanoemulsions is influenced by the size and sterics of the hydrophilic (A) block of the polymer amphiphiles. In most cases, longer A blocks produce larger initial nanoemulsions. This is particularly evident when considering the P(EtOx) series in which P($EtOx_{30}$-*b*-$NonOx_{10}$) (**11**) is initially 200 nm, while both P($EtOx_{90}$-*b*-$NonOx_{10}$) (**12**) and P($EtOx_{90}$-*b*-$NonOx_{30}$) (**13**) are 300 and 320, nm respectively. The commercial and P(MeOx) follow this trend, while PEG_{n}-*b*-$NonOx_{10}$ display similar initial sizes but with large dispersities.

The stability of the droplets over 30 days can be attributed to the HLB of the polymer. The P(MeOx) diblock polymers (**5–8**) and P(EtOx) (**11–13**) display this trend. As the ratio increases from 3:1 [P($MeOx_{30}$-*b*-$NonOx_{10}$) (**5**)] to 6:1 [P($MeOx_{60}$-*b*-$NonOx_{10}$) (**6**)] and 9:1 [P($MeOx_{90}$-*b*-$NonOx_{10}$) (**7**)], the change in volume of the droplets over 30 days increases from 1.5×10^7 to 2.75×10^7 nm^3. However, when the ratio returns to 3:1 with P($MeOx_{90}$-*b*-$NonOx_{30}$) (**8**), the droplets display similar stability to **5**. This holds true for the P(EtOx) series as well in which **11** and **13** have a 3:1 ratio.

The retention of payload is determined by the size of the hydrophilic (A) block and the molecular identity of the A block. Both of these factors determine the overall hydrophilicity of the A block. P(MeOx) is more hydrophilic than PEG, which is more hydrophilic than P(EtOx). This is displayed with the commercial polymers in which the long PEG TBCs (**1** and **2**) display superior retention (<10% release over 14 days) compared to shorter diblock Zonyl polymers (**3** and **4**). In addition, all P(MeOx) polymers retain 80% of the fluorous coumarin over 14 days compared to the P(EtOx) polymers that retain ~50% of the fluorous coumarin after 3 days. The PEG_{n}-*b*-$NonOx_{10}$ polymers showcase that hydrophilicity can also be tuned through increasing the length of the hydrophilic block, in which **16** retains 80% of the cargo after 3 days, but **14** only retains 20% after 3 days.

Lastly, the cellular endocytosis and the protein adsorption are controlled by the molecular identity and the polymer architecture. The more hydrophilic polymers, the commercial and P(MeOx) polymers, undergo clathrin-mediated endocytosis while the more hydrophobic polymers, P(EtOx) and PEG_{n}-*b*-$NonOx_{10}$, are internalized by several mechanisms. Overall, the TBCs behave similarly to the DBCs, with slight differences in the identity of the proteins that are adsorbed.

This study provides a necessary background on the structure–property relationship of polymer amphiphiles for the stabilization of PFC nanoemulsions. Through the identification of four criteria—hydrophilic block sizes, HLB, molecular identity, and polymer architecture—the ideal nanomaterial can be more easily realized. Future work involves combining the amphiphile design rules established here with fluorous-tagged therapeutics to enable efficient and personalized drug delivery with nanoemulsions.

EXPERIMENTAL SECTION

General Polymer Synthesis.

Polymers 5–13.—To a flame dried microwave vial, MeCN (1.2 mL, anhydrous) and 2-methyl-2-oxazoline (S1) or 2-ethyl-2-oxazoline (S2) were added. After brief mixing, methyl triflate (MeOTf) was added, and the mixture was heated at 140 °C in the microwave. The block lengths were controlled via the monomer to initiator ratio and reaction time.[45,46] Following completion of the first block, 2-nonyl-2-oxazoline (S3) was added under N_2 and heated to 140 °C. After completion of the second block for TBCs (**9–10**), 2-methyl-2-oxazoline (S1) was added under N_2 and heated to 140 °C followed by quenching with excess Milli-Q water, or for DBCs (**5–8** and **11–13**), the reaction was quenched with excess Milli-Q water. After stirring overnight, the reaction mixture was evaporated to dryness to yield a crude polymer as a white solid. Polymers were purified by dialysis against 1:1 dichloromethane (DCM)/MeOH (vol %) overnight, collected, and evaporated to dryness.

Polymers 14–16.—To a flame-dried microwave vial, MeCN and PEG$_n$-tosylate (**S4–S6**) were added. After brief mixing, 2-nonyl-2-oxazoline (S3) was added, and the mixture was heated at 140 °C in the microwave. After polymerization was complete, the reaction was quenched with Milli-Q water (excess). After stirring overnight, the reaction mixture was evaporated to dryness to yield a crude polymer as a white solid. Polymers were purified by dissolving in DCM and washing against water, then further dialyzing against MeOH overnight, collecting and evaporating to dryness.

General Nanoemulsion Formation Procedure.

The polymer surfactant (5.6 mg, 2.8 wt %) was dissolved in a co-solvent (20 μL, DMF, MeOH, or THF) and sonicated in a bath sonicated (~15 min) until fully dissolved, at which point 7:3 PFD/PFTPA (10 vol %, 20 μL) was added, followed by PBS buffer pH 7.4 (200 μL). Pluronic F-68 (**1**), Pluronic F-127 (**2**), Zonyl FSO (**3**), and Zonyl FSN (**4**) required no co-solvent. P(MeOx$_x$-*b*-NonOxy-*b*-MeOx$_z$) (**5–10**), P(EtOx$_x$-*b*-NonOx$_y$) (**11–13**), and PEG$_{1K}$-*b*-NonOx$_{10}$ (**14**) were dissolved in DMF. PEG$_{2K}$-*b*-NonOx$_{10}$ (**15**) and PEG$_{5K}$-*b*-NonOx$_{10}$ (**16**) were dissolved in THF and MeOH, respectively. The mixture was sonicated at 35% amplitude for 90 s at 0 °C on a QSonica (Q125) sonicator. For P(EtOx$_x$-*b*-NonOx$_y$) (**11–13**) and PEG$_n$-*b*-NonOx$_m$ (**14–16**) polymers, the mixture was sonicated at 35% amplitude for 90 s pulsed on for 2 s and off for 10 s at 0 °C. Sonication was performed by lowering the probe directly at the liquid-liquid interface of the two immiscible solvents. To remove cosolvents, emulsions are washed by centrifugation (5.6g, 3 min, 2×).

Nanoemulsion Size Analysis.

The bulk emulsion solution was diluted in Milli-Q H_2O (20 μL of emulsions in 2 mL of Milli-Q H_2O) in a plastic 1 cm cuvette. The size was analyzed with a Malvern Zetasizer Nano DLS. Data are representative of three replicate measurements. Size error bars represent the product of the dispersity and the z-average of the measurements.

Payload Release Experiment.

PFC nanoemulsions (**1–16**) containing fluorous coumarin **17** were prepared by dissolving coumarin in acetone to make a stock solution (2.3 mg/mL). Coumarin **17** (0.05 mg, 0.04 μ mol, 20 μL) was then aliquoted into Eppendorf tubes, and the acetone was dried. Once dried, PFCs (7:3 PFD/PFTPA, 20 μL) were added to dissolve the coumarin, and deionized water (200 μL) was added. Separately, the polymers were dissolved with the required co-solvent. The PFC/water mixture was placed on the sonication probe, and immediately before starting the probe, the polymer solution (see General Nanoemulsion Formation Procedure) was added. The mixture was sonicated for 90 s either continuously or pulsed, as described in the general nanoemulsion formation procedure. Immediately after formation, emulsion solution (40 μL) was diluted with PBS (960 μL), and 1-octanol (500 μL) was layered on top of the water and placed on an orbital rocker at 40 rpm.

1-Octanol (200 μL) was removed with a syringe (250 μL Hamilton) at 3 h, 1 day, 3 days, 7 days, 10 days, and 14 days, and the fluorescence was measured in a 0.3 cm quartz cuvette. After measurement, 1-octanol was carefully replaced to minimize loss during transfer and placed back on the rocker until the next measurement.

The control was fluorous coumarin **17** (3.2 μL, 0.007 mg, 6 nmol) dissolved in 1-octanol (500 μL) directly, and was bath sonicated for 10 min to dissolve. This is the amount of fluorous coumarin that is expected to come into contact with 1-octanol after the emulsions were diluted with PBS.

Photoluminescence spectra were obtained on a HORIBA Instruments PTI QuantaMaster Series fluorometer.

General Cell Culture Procedures.

RAW264.7 cells (ATCC cat # TIB-71) were cultured in DMEM (Life Technologies, cat # 11995073) supplemented with 10% FBS (Corning, lot# 35016109) and 1% PenStrep (Life Technologies, cat# 15070063). Cells were washed with PBS or PBS supplemented with 1% FBS (FACS buffer). Cells were incubated at 37 °C, 5% CO_2, during treatments and throughout culturing, in HERACell 150i CO2 incubators. Cells were pelleted through use of a Sorvall ST 40R centrifuge. All cell work was performed in 1300 Series A2 biosafety cabinets.

For cell viability experiments, following incubation, cells were washed three times by centrifugation (526*g*, 3 min, 4 °C). Propidium iodide (PI) solution (2 μL of 1 mg/mL in PBS) was added to each well. Cells treated with PI were transferred to FACS tubes with a final volume of 200 μL FACS buffer (PBS + 1% FBS). Cells were incubated on ice for 15 min prior to flow cytometry measurement. PI fluorescence was measured on the FL2 channel. Data were analyzed by splitting the population at 10^2 as a live/dead line. Flow cytometry was performed on a BD Biosciences FACSCalibur equipped with 488 and 635 nm lasers. For assessment of the statistical significance of differences, a one-tailed Student's *t*-test assuming an unequal sample variance was employed.

For inhibition experiments, media were removed and replaced with DMEM (100 μL of either basal or complete) and inhibitors NaN_3 (10 mM), chlorpromazine (60 μM), wortmannin (0.4 μM), MβCD (20 μM), and chloroquine (100 μM). After 1 h, emulsions (10 μL) were added to the cells and incubated for 3 h at 37 °C, 5% CO_2. For 4 °C, emulsions were added to cells and placed at 4 °C for 1 h to prevent excessive cell death. Cells were then washed with media 3×, sterile lithium chloride buffer [LiCl: 0.25 M LiCl, 1 mM ethylenediaminetetraacetic acid (EDTA), 10 mM Tris-HCl] 3×, and PBS 1×, then lifted with trypsin, and transferred to a v-bottom 96-well plate. Note that PFC nanoemulsions are dense and settle on top of the cells. Slight rocking was necessary to successfully remove excess emulsions. Cells were washed by centrifugation (526*g*, 3 min, 2×) and resuspended in FACS buffer (PBS + 1% FBS) to a final volume of 200 μL. Uptake was analyzed by the FL2 channel on a FACSCalibur flow cytometer. A total of 15,000 cells were collected per sample. Each emulsion was normalized to one of the replicates in the samples with no inhibitors present. Error bars represent the standard deviation of three replicate experiments.

Supplementary Material

Refer to Web version on PubMed Central for supplementary material.

ACKNOWLEDGMENTS

This work was funded by the Alfred P. Sloan Award (FG-2018-10855) and Hellman Fellows Award to E.M.S. D.A.E. was supported by the T32 training grant from the National Institute of General Medical Sciences (NIH, grant no. 5T32GM067555-12). D.A.E. and R.A.D. were supported by the Majeti-Alapati Fellowship and the Saul Winstein Fellowships. C.W. was supported by the Lorraine H. and Masuo Toji Fund Summer Research Fellowship. J.O.C. was supported by the Raymond and Dorothy Wilson Research Fellowship and the Lau Family via the URSP Undergraduate Research Fellowship. A.J.T. was supported by a grant from the National Science Foundation awarded to Santa Monica College (NSF, grant no. 1928737). NMR data were obtained on instruments funded by the National Science Foundation (NSF, grant no. MRI CHE-1048804). We thank the Maynard group for use of equipment.

ABBREVIATIONS

BSA	bovine serum albumin
βME	β-mercaptoethanol
DBC	diblock copolymer
DCM	dichloromethane
DLS	dynamic light scattering
DMEM	Dulbecco’s modified Eagle media
DMF	dimethyl formamide
DMSO	dimethyl sulfoxide
EDTA	ethylenediaminetetraacetic acid
EtOH	ethanol

FACS	fluorescence activated cell sorting
FBS	fetal bovine serum
HLB	hydrophilic/lipophilic balance
HSA	human serum albumin
LiCl	lithium chloride
MβCD	methyl-β-cyclodextrin
MeCN	acetonitrile
MeOH	methanol
MeOTf	methyl triflate
NaN_3	sodium azide
NMR	nuclear magnetic resonance
P(EtOx)	poly(2-ethyloxazoline)
P(MeOx)	poly(2-methyloxazoline)
P(NonOx)	poly(2-nonyloxazoline)
PBS	phosphate buffered saline
PDI	polydispersity index
PEG	poly(ethylene glycol)
PenStrep	penicillin streptomycin
PFC	perfluorocarbon
PFCE	perfluoro-15-crown-5-ether
PFD	perfluorodecalin
PFOB	perfluorooctyl bromide
PFTPA	perfluorotripropylamine
PMMA	poly(methyl-methacrylate)
POx	poly(2-oxazoline)
SDS-PAGE	sodium dodecyl sulfate polyacrylamide gel electrophoresis
SEC	size exclusion chromatography
TBC	triblock copolymer
THF	tetrahydrofuran

Tris-HCl	Tris(hydroxymethyl)aminomethane hydrochloride

REFERENCES

(1). Shi J; Kantoff PW; Wooster R; Farokhzad OC Cancer Nanomedicine: Progress, Challenges and Opportunities. Nat. Rev. Cancer 2017, 17, 20–37. [PubMed: 27834398]

(2). Bobo D; Robinson KJ; Islam J; Thurecht KJ; Corrie SR Nanoparticle-Based Medicines: A Review of FDA-Approved Materials and Clinical Trials to Date. Pharm. Res 2016, 33, 2373–2387. [PubMed: 27299311]

(3). De Jong WH; Borm BJA Drug Delivery and Nanoparticles: Applications and Hazards. Int. J. Nanomed 2008, 3, 133–149.

(4). Van Haute D; Liu AT; Berlin JM Coating Metal Nanoparticle Surfaces with Small Organic Molecules Can Reduce Nonspecific Cell Uptake. ACS Nano 2018, 12, 117–127. [PubMed: 29261281]

(5). Linares J; Matesanz MC; Vila M; Feito MJ; Gonçalves G; Vallet-Regí M; Marques PAAP; Portolés MT Endocytic Mechanisms of Graphene Oxide Nanosheets in Osteoblasts, Hepatocytes and Macrophages. ACS Appl. Mater. Interfaces 2014, 6, 13697–13706. [PubMed: 24979758]

(6). Francia V; Yang K; Deville S; Reker-smit C; Nelissen I; Salvati A Corona Composition Can Affect the Mechanisms Cells Use to Internalize Nanoparticles. ACS Nano 2019, 13, 11107–11121. [PubMed: 31525954]

(7). Chithrani BD; Ghazani AA; Chan WCW Determining the Size and Shape Dependence of Gold Nanoparticle Uptake into Mammalian Cells. Nano Lett. 2006, 6, 662–668. [PubMed: 16608261]

(8). Su G; Zhou H; Mu Q; Zhang Y; Li L; Jiao P; Jiang G; Yan B Effective Surface Charge Density Determines the Electrostatic Attraction between Nanoparticles and Cells. J. Phys. Chem. C 2012, 116, 4993–4998.

(9). Beduneau A; Ma Z; Grotepas CB; Kabanov A; Rabinow BE; Gong N; Mosley RL; Dou H; Boska MD; Gendelman HE Facilitated Monocyte-Macrophage Uptake and Tissue Distribution of Superparmagnetic Iron-Oxide Nanoparticles. PLoS One 2009, 4, No. e4343. [PubMed: 19183814]

(10). Albanese A; Tang PS; Chan WCW The Effect of Nanoparticle Size, Shape, and Surface Chemistry on Biological Systems. Annu. Rev. Biomed. Eng 2012, 14, 1–16. [PubMed: 22524388]

(11). Bai X; Liu F; Liu Y; Li C; Wang S; Zhou H; Wang W; Zhu H; Winkler DA; Yan B Toward a Systematic Exploration of Nano-Bio Interactions. Toxicol. Appl. Pharmacol. 2017, 323, 66–73. [PubMed: 28344110]

(12). Hauck TS; Ghazani AA; Chan WCW Assessing the Effect of Surface Chemistry on Gold Nanorod Uptake, Toxicity, and Gene Expression in Mammalian Cells. Small 2008, 4, 153–159. [PubMed: 18081130]

(13). Vertegel AA; Siegel RW; Dordick JS Silica Nanoparticle Size Influences the Structure and Enzymatic Activity of Adsorbed Lysozyme. Langmuir 2004, 20, 6800–6807. [PubMed: 15274588]

(14). Durán N; Silveira CP; Durán M; Martinez DST Silver Nanoparticle Protein Corona and Toxicity: A Mini-Review. J. Nanobiotechnol 2015, 13, 55.

(15). Lu F; Wu S-H; Hung Y; Mou C-Y Size Effect on Cell Uptake in Well-Suspended, Uniform Mesoporous Silica Nanoparticles. Small 2009, 5, 1408–1413. [PubMed: 19296554]

(16). Barenholz Y Doxil—The First FDA-Approved Nano-Drug: Lessons Learned. J. Controlled Release 2012, 160, 117–134.

(17). Peer D; Karp JM; Hong S; Farokhzad OC; Margalit R; Langer R Nanocarriers as an Emerging Platform for Cancer Therapy. Nat. Nanotechnol 2007, 2, 751–760. [PubMed: 18654426]

(18). Tadros T; Izquierdo P; Esquena J; Solans C Formation and Stability of Nano-Emulsions. Adv. Colloid Interface Sci 2004, 108–109, 303–318.

(19). Gupta A; Eral HB; Hatton TA; Doyle PS Nanoemulsions: Formation, Properties and Applications. Soft Matter 2016, 12, 2826–2841. [PubMed: 26924445]

(20). Hörmann K; Zimmer A Drug Delivery and Drug Targeting with Parenteral Lipid Nanoemulsions—A Review. J. Controlled Release 2016, 223, 85–98.

(21). Takino T; Konishi K; Takakura Y; Hashida M Long Circulating Emulsion Carrier Systems for Highly Lipophilic Drugs. Biol. Pharm. Bull 1994, 17, 121–125. [PubMed: 8148799]

(22). Day RA; Estabrook DA; Logan JK; Sletten EM Fluorous Photosensitizers Enhance Photodynamic Therapy with Perfluorocarbon Nanoemulsions. Chem. Commun 2017, 53, 13043–13046.

(23). Gladysz JA; Jurisch M Structural, Physical and Chemical Properties of Fluorous Compounds; Springer: Berlin, Heidelberg, 2011; Vol. 308, pp 1–23.

(24). Krafft MP; Riess JG Perfluorocarbons: Life Sciences and Biomedical Uses Dedicated to the memory of Professor Guy Ourisson, a true RENAISSANCE man. J. Polym. Sci., Part A: Polym. Chem 2007, 45, 1185–1198.

(25). Riess JG Oxygen Carriers ("Blood Substitutes")Raison d'Etre, Chemistry, and Some Physiology Blut ist ein ganz besondrer Saft1. Chem. Rev 2001, 101, 2797–2920. [PubMed: 11749396]

(26). Tirotta I; Dichiarante V; Pigliacelli C; Cavallo G; Terraneo G; Bombelli FB; Metrangolo P; Resnati G 19F Magnetic Resonance Imaging (MRI): From Design of Materials to Clinical Applications. Chem. Rev 2015, 115, 1106–1129. [PubMed: 25329814]

(27). Janjic JM; Ahrens ET Fluorine-Containing Nanoemulsions for MRI Cell Tracking. Wiley Interdiscip. Rev.: Nanomed. Nanobiotechnol 2009, 1, 492–501.

(28). Tirotta I; Mastropietro A; Cordiglieri C; Gazzera L; Baggi F; Baselli G; Bruzzone MG; Zucca I; Cavallo G; Terraneo G; Baldelli Bombelli F; Metrangolo P; Resnati G A Superfluorinated Molecular Probe for Highly Sensitive in Vivo 19F-MRI. J. Am. Chem. Soc 2014, 136, 8524–8527. [PubMed: 24884816]

(29). Tran TD; Caruthers SD; Hughes M; Marsh JN; Cyrus T; Winter PM; Neubauer AM; Wickline SA; Lanza GM Clinical Applications of Perfluorocarbon Nanoparticles for Molecular Imaging and Targeted Therapeutics. Int. J. Nanomed 2007, 2, 515–526.

(30). Rapoport N; Nam K-H; Gupta R; Gao Z; Mohan P; Payne A; Todd N; Liu X; Kim T; Shea J; Scaife C; Parker DL; Jeong E-K; Kennedy AM Ultrasound-Mediated Tumor Imaging and Nanotherapy Using Drug Loaded, Block Copolymer Stabilized Perfluorocarbon Nanoemulsions. J. Controlled Release 2011, 153, 4–15.

(31). Patrick MJ; Janjic JM; Teng H; O'Hear MR; Brown CW; Stokum JA; Schmidt BF; Ahrens ET; Waggoner AS Intracellular PH Measurements Using Perfluorocarbon Nanoemulsions. J. Am. Chem. Soc 2013, 135, 18445–18457. [PubMed: 24266634]

(32). Janjic JM; Srinivas M; Kadayakkara DKK; Ahrens ET Self-Delivering Nanoemulsions for Dual Fluorine-19 MRI and Fluorescence Detection. J. Am. Chem. Soc 2008, 130, 2832–2841. [PubMed: 18266363]

(33). Kaneda MM; Sasaki Y; Lanza GM; Milbrandt J; Wickline SA Mechanisms of Nucleotide Trafficking during SiRNA Delivery to Endothelial Cells Using Perfluorocarbon Nanoemulsions. Biomaterials 2010, 31, 3079–3086. [PubMed: 20092889]

(34). Partlow KC; Lanza GM; Wickline SA Exploiting Lipid Raft Transport with Membrane Targeted Nanoparticles: A Strategy for Cytosolic Drug Delivery. Biomaterials 2008, 29, 3367–3375. [PubMed: 18485474]

(35). Gould SA; Rosen AL; Sehgal LR; Sehgal HL; Langdale LA; Krause LM; Rice CL; Chamberlin WH; Moss GS Fluosol-DA as a Red-Cell Substitute in Acute Anemia. N. Engl. J. Med 1986, 314, 1653–1656. [PubMed: 3713771]

(36). Viegas TX; Bentley MD; Harris JM; Fang Z; Yoon K; Dizman B; Weimer R; Mero A; Pasut G; Veronese FM Polyoxazoline: Chemistry, Properties, and Applications in Drug Delivery. Bioconjugate 2011, 22, 976–986.

(37). Hoogenboom R Poly(2-Oxazoline)s: A Polymer Class with Numerous Potential Applications. Angew. Chem., Int. Ed 2009, 48, 7978–7994.

(38). Estabrook DA; Ennis AF; Day RA; Sletten EM Controlling Nanoemulsion Surface Chemistry with Poly(2-Oxazoline) Amphiphiles. Chem. Sci 2019, 10, 3994–4003. [PubMed: 31015940]

(39). Feng H; Lu X; Wang W; Kang N-G; Mays J Block Copolymers: Synthesis, Self-Assembly, and Applications. Polymers 2017, 9, 494.

(40). Tadros T Principles of Emulsion Stabilization with Special Reference to Polymeric Surfactants. J. Cosmet. Sci 2006, 57, 153–169. [PubMed: 16688378]

(41). Hoogenboom R; Wiesbrock F; Huang H; Leenen MAM; Thijs HML; Van Nispen SFGM; Van Der Loop M; Fustin C-A; Jonas AM; Gohy J-F; Schubert US Microwave-Assisted Cationic Ring-Opening Polymerization of 2-Oxazolines: A Powerful Method for the Synthesis of Amphiphilic Triblock Copolymers. Macromolecules 2006, 39, 4719–4725.

(42). Lava K; Verbraeken B; Hoogenboom R Poly(2-Oxazoline)s and Click Chemistry: A Versatile Toolbox toward Multi-Functional Polymers. Eur. Polym. J 2015, 65, 98–111.

(43). Castro CI; Briceño JC Perfluorocarbon-Based Oxygen Carriers: Review of Products and Trials. Artif. Organs 2010, 34, 622–634. [PubMed: 20698841]

(44). Duncanson WJ; Arriaga LR; Ung WL; Kopechek JA; Porter TM; Weitz DA Microfluidic Fabrication of Perfluorohexane-Shelled Double Emulsions for Controlled Loading and Acoustic-Triggered Release of Hydrophilic Agents. Langmuir 2014, 30, 13765–13770. [PubMed: 25340527]

(45). Hannah AS; VanderLaan D; Chen Y-S; Emelianov SY Photoacoustic and Ultrasound Imaging Using Dual Contrast Perfluorocarbon Nanodroplets Triggered by Laser Pulses at 1064 Nm. Biomed. Opt. Express 2014, 5, 3042–3053. [PubMed: 25401018]

(46). Spence RK; Norcross ED; Costabile J; Mccoy S; Cernaianu AC; Alexander JB; Pello MJ; Atabek U; Camishion RC; Norcross ED; Costabile J; Mccoy S; Aurel C Perfluorocarbons as Blood Substitutes: The Early Years: Experience with Fluosol DA-20 % in The 1980s. Artif. Cell Blood Substit. Biotechnol 1994, 22, 955–963.

(47). Barres AR; Molugu SK; Stewart PL; Mecozzi S Droplet Core Intermolecular Interactions and Block Copolymer Composition Heavily Influence Oil-In-Water Nanoemulsion Stability. Langmuir 2019, 35, 12765–12772. [PubMed: 31532686]

(48). Levin A; Mason TO; Adler-Abramovich L; Buell AK; Meisl G; Galvagnion C; Bram Y; Stratford SA; Dobson CM; Knowles TPJ; Gazit E Ostwald's Rule of Stages Governs Structural Transitions and Morphology of Dipeptide Supramolecular Polymers. Nat. Commun 2014, 5, 5219. [PubMed: 25391268]

(49). Tadros TF Emulsion Formation and Stability; Wiley-VCH: United Kingdom, 2013.

(50). Lowe KC Perfluorinated Blood Substitutes and Artificial Oxygen Carriers. Blood Rev. 1999, 13, 171–184. [PubMed: 10527269]

(51). Sletten EM; Swager TM Readily Accessible Multifunctional Fluorous Emulsions. Chem. Sci 2016, 7, 5091. [PubMed: 30155158]

(52). Sletten EM; Swager TM Fluorofluorophores: Fluorescent Fluorous Chemical Tools Spanning the Visible Spectrum. J. Am. Chem. Soc 2014, 136, 13574–13577. [PubMed: 25229987]

(53). Miller MA; Sletten EM A General Approach to Biocompatible Branched Fluorous Tags for Increased Solubility in Perfluorocarbon Solvents. Org. Lett 2018, 20, 6850–6854. [PubMed: 30354161]

(54). Boija E; Johansson G Interactions between Model Membranes and Lignin-Related Compounds Studied by Immobilized Liposome Chromatography. Biochim. Biophys. Acta, Biomembr 2006, 1758, 620–626.

(55). Delmas T; Piraux H; Couffin A-C; Texier I; Vinet F; Poulin P; Cates ME; Bibette J How to Prepare and Stabilize Very Small Nanoemulsions. Langmuir 2011, 27, 1683–1692. [PubMed: 21226496]

(56). Allen C; Dos Santos N; Gallagher R; Chiu GNC; Shu Y; Li WM; Johnstone SA; Janoff AS; Mayer LD; Webb MS; Bally MB Controlling the Physical Behavior and Biological Performance of Liposome Formulations through Use of Surface Grafted Poly(Ethylene Glycol). Biosci. Rep. 2002, 22, 225–250. [PubMed: 12428902]

(57). Di Marzio L; Marianecci C; Cinque B; Nazzarri M; Cimini AM; Cristiano L; Cifone MG; Alhaique F; Carafa M PH-Sensitive Non-Phospholipid Vesicle and Macrophage-like Cells: Binding, Uptake and Endocytotic Pathway. Biochim. Biophys. Acta, Biomembr 2008, 1778, 2749–2756.

(58). Almalik A; Karimi S; Ouasti S; Donno R; Wandrey C; Day PJ; Tirelli N Hyaluronic Acid (HA) Presentation as a Tool to Modulate and Control the Receptor-Mediated Uptake of HA-Coated Nanoparticles. Biomaterials 2013, 34, 5369–5380. [PubMed: 23615561]

(59). Chithrani BD; Chan WCW Elucidating the Mechanism of Cellular Uptake and Removal of Protein-Coated Gold Nanoparticles of Different Sizes and Shapes. Nano Lett. 2007, 7, 1542–1550. [PubMed: 17465586]

(60). Misinzo G; Delputte PL; Nauwynck HJ Inhibition of Endosome-Lysosome System Acidification Enhances Porcine Circovirus 2 Infection of Porcine Epithelial Cells. J. Virol 2008, 82, 1128–1135. [PubMed: 18032516]

(61). Wang LH; Rothberg KG; Anderson RG Mis-Assembly of Clathrin Lattices on Endosomes Reveals a Regulatory Switch for Coated Pit Formation. J. Cell Biol 1993, 123, 1107–1117. [PubMed: 8245121]

(62). Konradi R; Acikgoz C; Textor M Polyoxazolines for Nonfouling Surface Coatings—A Direct Comparison to the Gold Standard PEG. Macromol. Rapid Commun 2012, 33, 1663–1676. [PubMed: 22996913]

(63). Konradi R; Pidhatika B; Mu A; Textor M Poly-2-Methyl-2-Oxazoline: A Peptide-like Polymer for Protein-Repellent Surfaces. Langmuir 2008, 24, 613–616. [PubMed: 18179272]

(64). Tong J; Luxenhofer R; Yi X; Jordan R; Kabanov AV Protein Modification with Amphiphilic Block Copoly (2-Oxazoline)s as a New Platform for Enhanced Cellular Delivery. Mol. Pharm 2010, 7, 984–992. [PubMed: 20550191]

(65). Woodle MC; Engbers CM; Zalipsky S New Amphipatic Polymer—Lipid Conjugates Forming Long-Circulating Reticuloendothelial System-Evading Liposomes. Bioconjugate Chem. 1994, 5, 493–496.

(66). Wilson P; Ke PC; Davis TP; Kempe K Poly(2-Oxazoline)-Based Micro- and Nanoparticles: A Review. Eur. Polym. J 2017, 88, 486–515.

(67). Koshkina O; Westmeier D; Lang T; Bantz C; Hahlbrock A; Würth C; Resch-genger U; Braun U; Thiermann R; Weise C; Eravci M; Mohr B; Schlaad H; Stauber RH; Docter D; Bertin A; Maskos M Tuning the Surface of Nanoparticles: Impact of Poly (2-Ethyl-2-Oxazoline) on Protein Adsorption in Serum and Cellular Uptake. Macromol. Biosci 2016, 16, 1287–1300. [PubMed: 27281039]

(68). Barz M; Luxenhofer R; Zentel R; Vicent MJ Overcoming the PEG-Addiction: Well-Defined Alternatives to PEG, from Structure–Property Relationships To Better Defined Therapeutics. Polym. Chem 2011, 2, 1900–1918.

(69). Suk JS; Xu Q; Kim N; Hanes J; Ensign LM; Sciences H; Sciences M PEGylation as a Strategy for Improving Nanoparticle-Based Drug and Gene Delivery. Adv. Drug Delivery Rev 2016, 99, 28–51.

(70). Schöttler S; Becker G; Winzen S; Steinbach T; Mohr K; Landfester K; Mailänder V; Wurm FR Protein Adsorption Is Required for Stealth Effect of Poly(Ethylene Glycol)- and Poly-(Phosphoester)- Coated Nanocarriers. Nat. Nanotechnol 2016, 11, 372–377. [PubMed: 26878141]

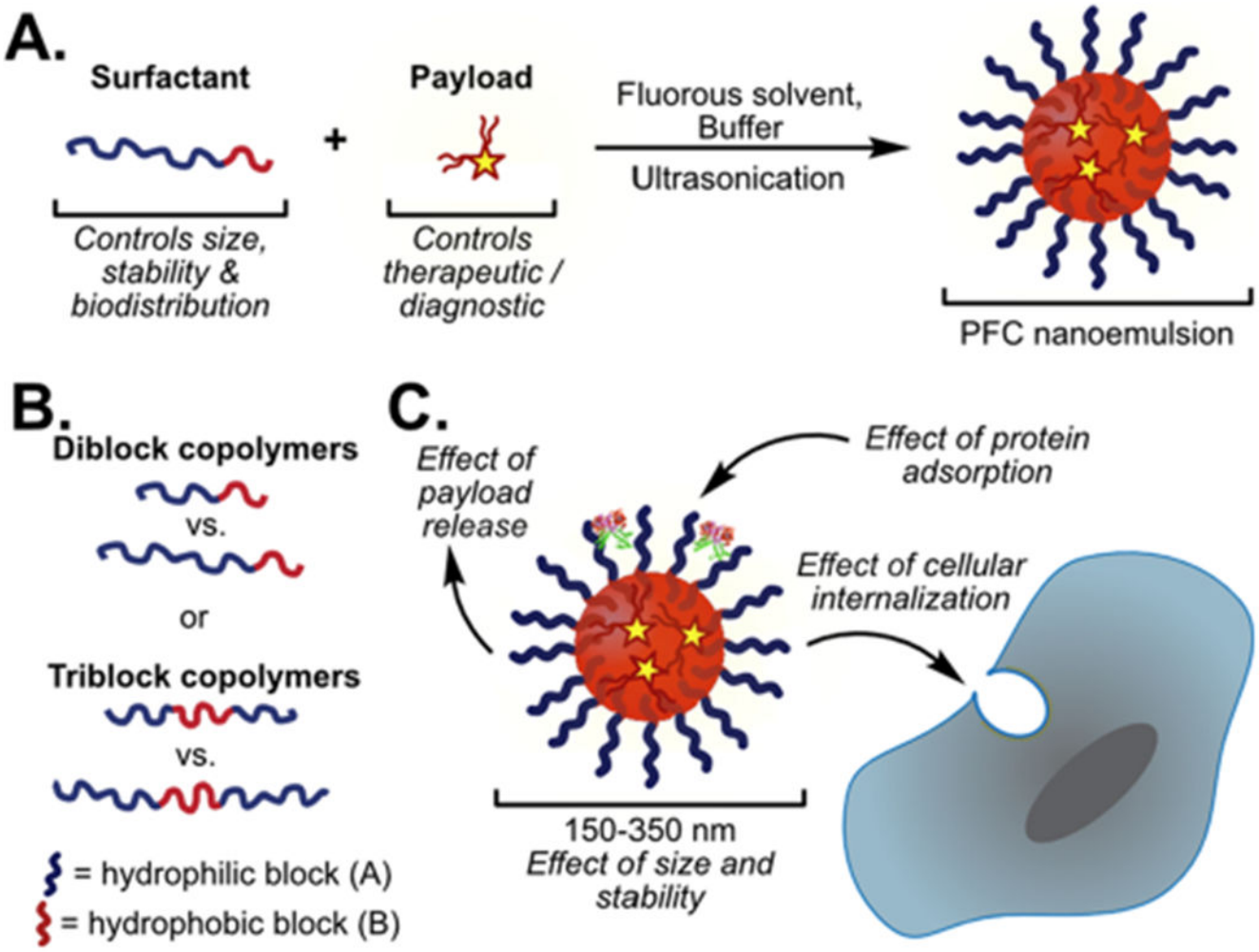

Figure 1.

(A) One step formulation of PFC nanoemulsions stabilized by polymer surfactants containing fluorous soluble payloads. (B) Polymer amphiphile block length and architecture dictate properties. (C) Surfactants dictate the size, stability, protein adsorption, and route of cellular endocytosis of PFC nanoemulsions.

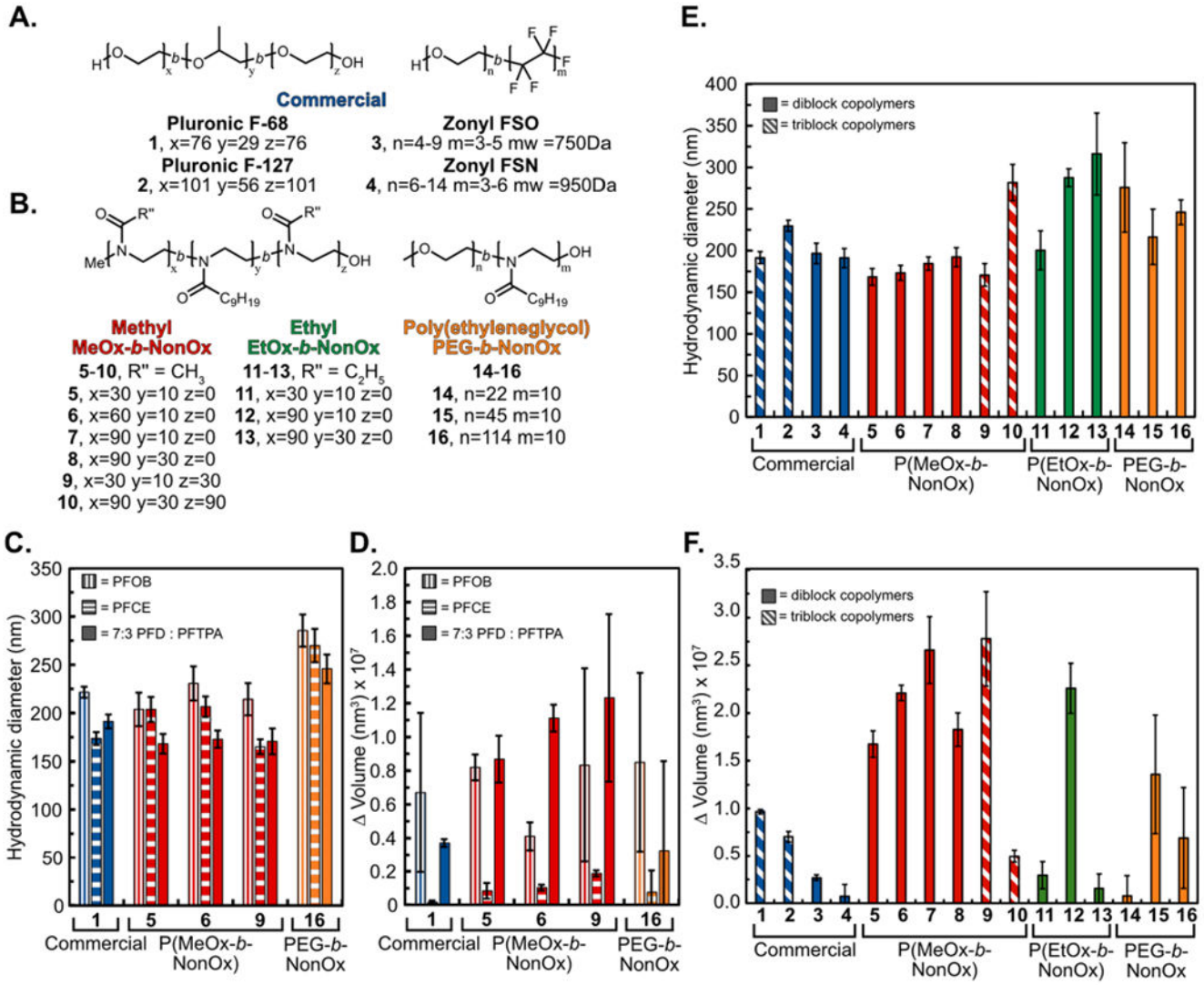

Figure 2.

(A,B) Library of amphiphilic DBCs and TBCs. Commercial (blue), P(MeOx) (red), P(EtOx) (green), and PEG-*b*-NonOx (orange) (**1–16**). (C) Initial size distribution of PFC nanoemulsions containing differing fluorous solvents [perfluorooctyl bromide (PFOB), vertical stripes; perfluoro-15-crown-5-ether (PFCE), horizontal stripes; 7:3 perfluorodecalin/perfluorotripropylamine, (PFD/PFTPA), solid] stabilized by **1** (PF68), **5** [P($MeOx_{30}$-*b*-$NonOx_{10}$)], **6** [P($MeOx_{60}$-*b*-$NonOx_{10}$)], **9** [P($MeOx3_0$-*b*-$NonOx_{10}$-*b*-$MeOx_{30}$)], and **16** (PEG_{5K}-*b*-$NonOx_{10}$). (D) Change in volume over 14 days of PFC nanoemulsions shown in (C). (E) Initial size distributions of amphiphile stabilized 7:3 PFD/PFTPA PFC nanoemulsions. Nanoemulsions were prepared by sonication of a solution of 2.8 wt % surfactant with 10 vol % 7:3 PFD/PFTPA in phosphate buffered saline (PBS). Emulsions were diluted 1:1000 in deionized water prior to measurements by dynamic light scattering (DLS). Data represent the average of three independent samples; error bars represent the product of the dispersity and the *z*-average. (F) Change in volume over 30 days of emulsions

shown in (E). Data represent the average of three independent samples; error bars represent the standard deviation of three independent samples.

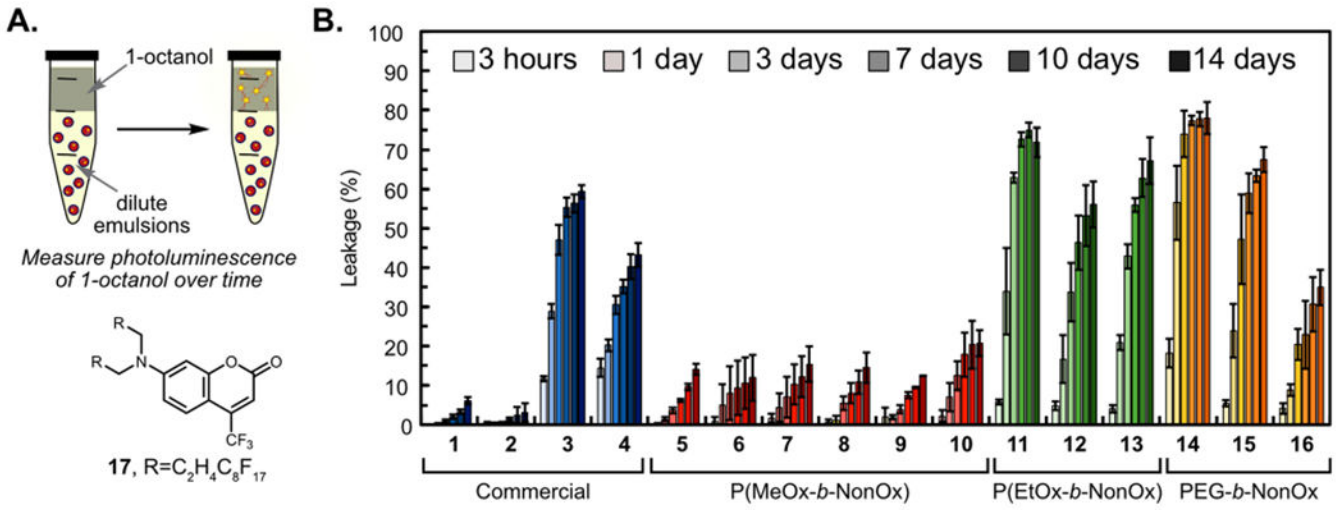

Figure 3.

(A) Schematic of the partition experiment to determine the degree of coumarin **17** leaching in the presence of 1-octanol, a cell-membrane mimic. (B) Normalized fluorescence at 500 nm of the 1-octanol layer representing the percentage of leached coumarin **17**. Fluorescence was normalized to a free control of **17** dissolved in 1-octanol. Bars represent the average of three independent samples, and error bars represent the standard deviation of three independent samples.

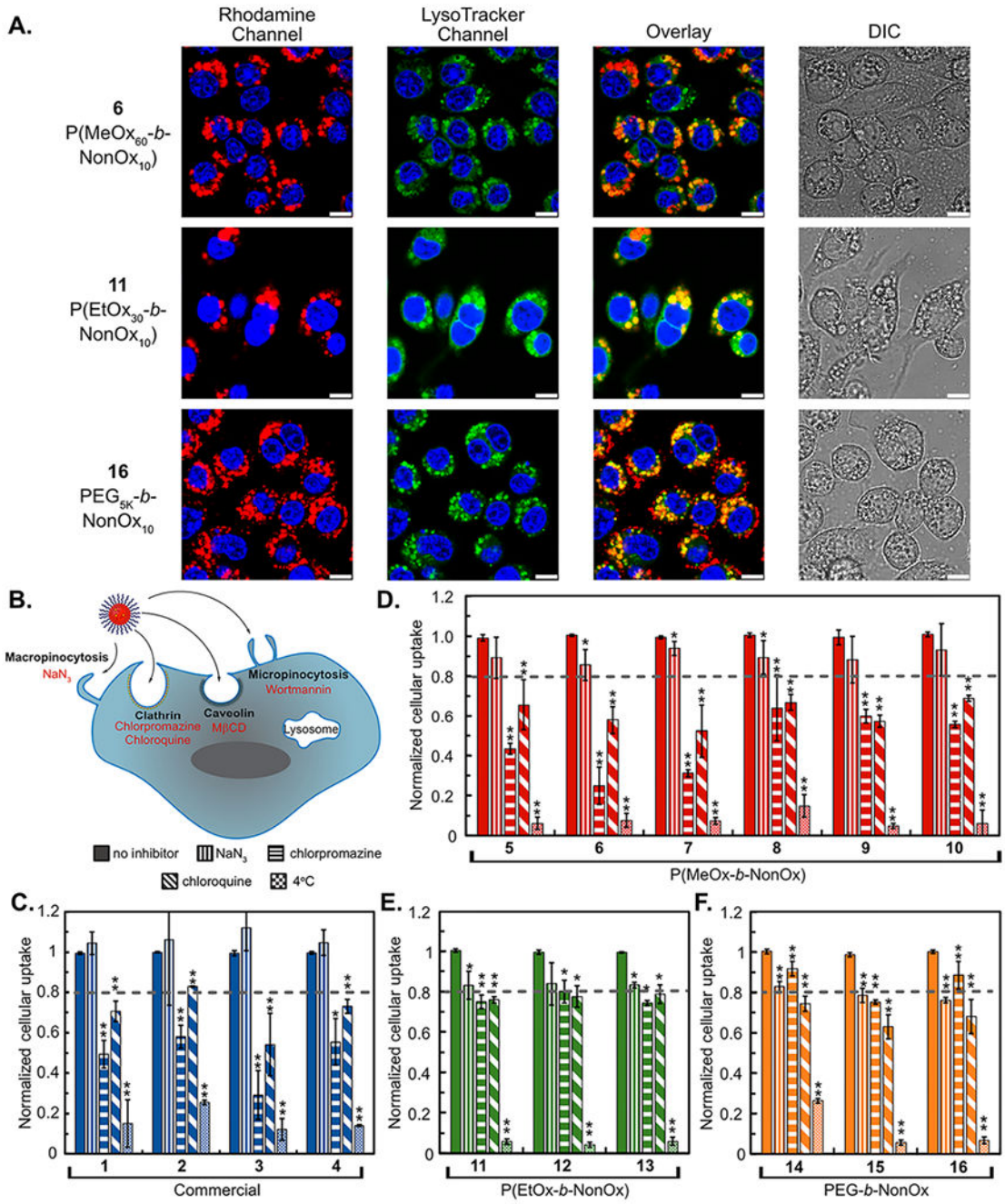

Figure 4.

(A) Confocal microscopy showing the uptake of PFC nanoemulsions. Emulsions contain fluorous rhodamine (red) visualized with 532 nm excitation. LysoTracker (green) visualized with 488 nm laser and nuclei stained with Hoescht (blue) visualized with 405 nm laser. Scale bar represents 7.5 μm. (B) Schematic of cellular uptake and the inhibitors used to inhibit each mechanism of endocytosis. (C–F) Fluorescence-activated cell sorting (FACS) analysis of the uptake of PFC nanoemulsions containing fluorous rhodamine. RAW264.7 cells were treated with inhibitors [NaN3 (10 mM), chlorpromazine (60 μM), chloroquine

(100 μM)] in basal media [Dulbecco's modified Eagle media (DMEM), 0% fetal bovine serum (FBS), 0% penicillin streptomycin (PenStrep)] for 1 h at 37 °C before addition of nanoemulsions and treatment for a further **3** h. Cells were washed and analyzed for fluorous rhodamine fluorescence. Data are the average of three replicate experiments performed in triplicates and normalized to cells treated with emulsions but no inhibitor (vertical stripes). Error bars represent the standard deviation. Significance is determined by one-tailed Student's *t*-test of unequal variance as compared to the no inhibitor samples. $p \leq 0.05$ *, $p \leq 0.005$ **.

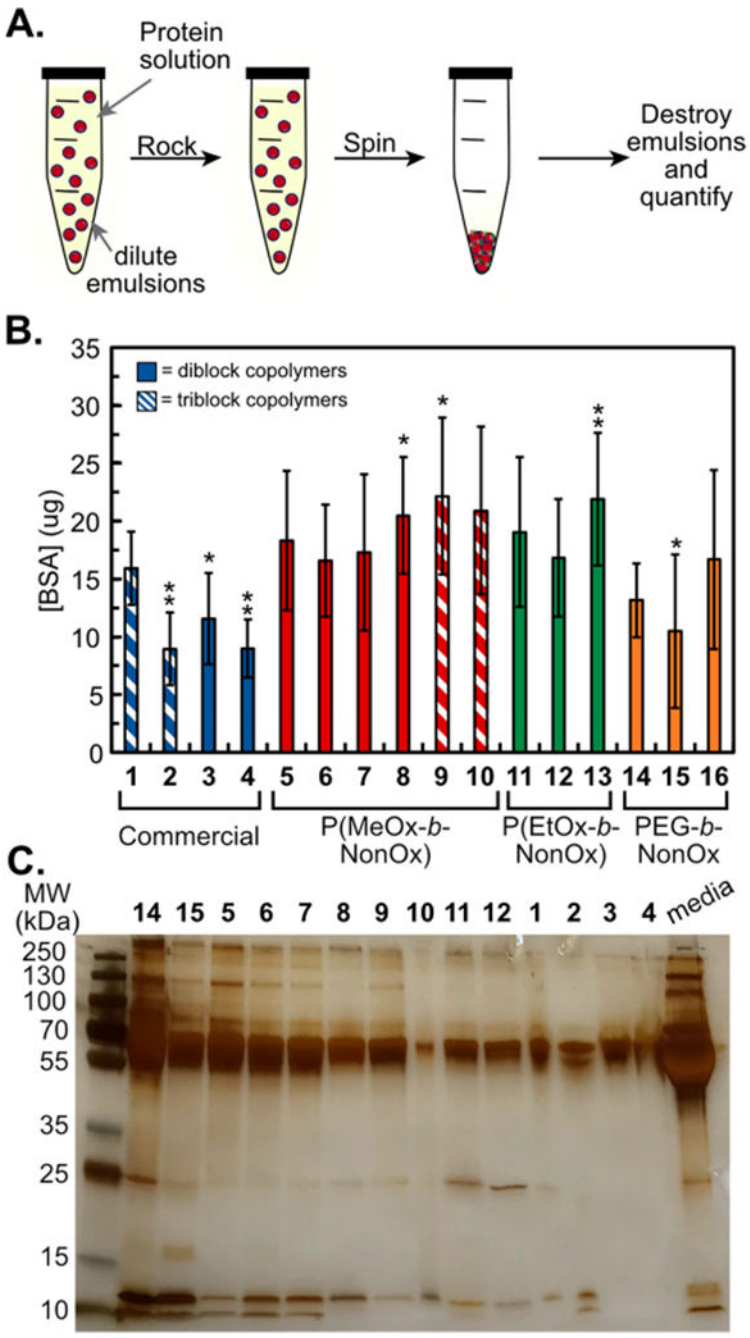

Figure 5.

(A) Schematic of protein adsorption analysis in which emulsions are rocked against a protein solution, washed, and quantified. (B) Bradford analysis of PFC nanoemulsions treated with 60 mg/mL BSA for 2 h at room temperature. Bars represent the average of three experiments, each done in triplicate. Error bars represent the standard deviation. Significance is determined by one tailed Studen's *t*-test of unequal variance as compared to Pluronic F-68 (**1**) $p < 0.05$ *, $p < 0.005$ **. (C) SDS-PAGE of PFC nanoemulsions treated

with complete media (DMEM, 10% FBS, and 1% PenStrep), for 2 h at room temperature. Protein was denatured, run on a 12% gel, and visualized with silver stain.

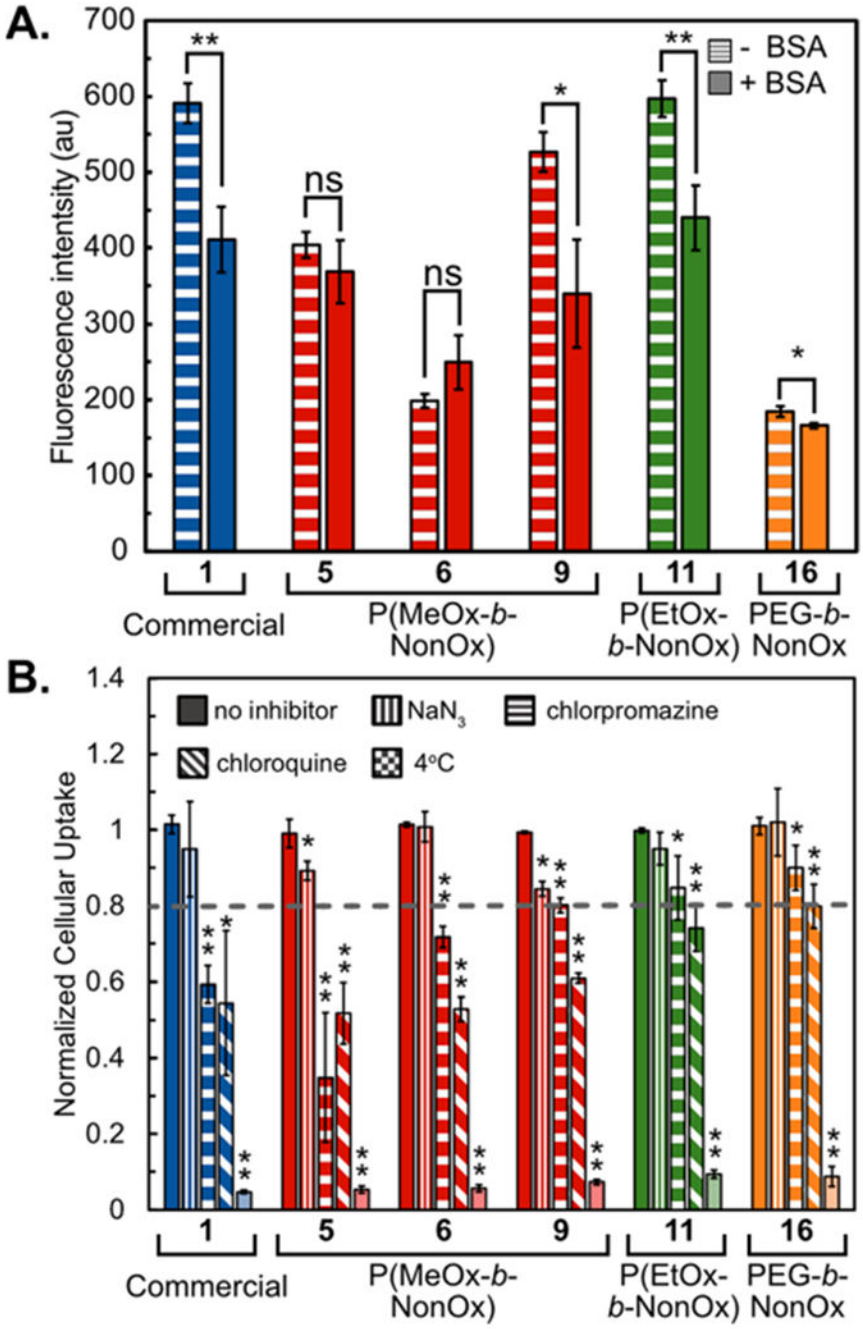

Figure 6.

(A) Comparative endocytosis of PFC nanoemulsions in the presence or absence of a protein corona (±BSA). PFC nanoemulsions were treated with 60 mg/mL BSA or PBS for 2 h at room temperature, washed by centrifugation 2× and added to cells (3 h, 37 °C, 5% CO_2). Fluorous rhodamine fluorescence was measured via FL2 channel by FACS. Bars represent the average of two replicate experiments performed in triplicates. Error bars represent the standard deviation. (B) FACS analysis of the uptake of PFC nanoemulsions containing fluorous rhodamine. RAW264.7 cells were treated with inhibitors [NaN_3 (10 mM),

chlorpromazine (60 μM), and chloroquine (100 μM)] in complete media (DMEM, 10% FBS, 1% PenStrep) for 1 h at 37 °C before addition of nanoemulsions and treatment for a further 3 h. Cells were washed and analyzed for fluorous rhodamine fluorescence. Data are the average of three replicate experiments performed in triplicates and normalized to cells treated with emulsions but no inhibitor. Error bars represent the standard deviation. One tailed Studen's *t*-test with unequal variance was performed in relation to no inhibitor. $p \leq 0.05$ *, $p \leq 0.01$ **.